Exceptional points of resonant states on a periodic slab

Amgad Abdrabou and Ya Yan Lu*
Department of Mathematics, City University of Hong Kong, Kowloon, Hong Kong, China

(Received 11 April 2018; published 12 June 2018)

A special kind of degeneracy, known as exceptional points (EPs), for resonant states on a dielectric periodic slab are investigated. Due to their unique properties, EPs have found important applications in lasing, sensing, unidirectional operations, etc. In general, EPs may appear in non-Hermitian eigenvalue problems, including those related to -parity-time-symmetric systems and those for open dielectric structures (due to the existence of radiation loss). In this paper, we study EPs on a simple periodic structure: a slab with a periodic array of gaps. By using an efficient numerical method, we calculate the EPs and study their dependence on geometric parameters. Analytic results are obtained for the limit as the periodic slab approaches a uniform one. Our work provides a simple platform for further studies concerning EPs on dielectric periodic structures, their unusual properties, and applications.

DOI: 10.1103/PhysRevA.97.063822

I. INTRODUCTION

In parameter-dependent eigenvalue problems of non-Hermitian operators, a special kind of degeneracy may occur at some particular values of the system parameters; that is, two or more eigenvalues coalesce and their corresponding eigenfunctions collapse into one single function. Such a spectral degeneracy is called an exceptional point (EP) [1]. EPs are interesting because they give rise to unusual physical phenomena in many systems related to non-Hermitian eigenvalue problems [2–8]. EPs are also central to quantum or classical parity-time-symmetric ($\mathcal{PT}$-symmetric) systems [9,10]. In these systems, an EP corresponds to a transition (also known as $\mathcal{PT}$-symmetry breaking) from a state with all real eigenvalues to a state with complex eigenvalues [11]. In recent years, $\mathcal{PT}$-symmetric optical systems have been intensively investigated. EPs have been observed in $\mathcal{PT}$-symmetric waveguides [12,13] and exploited in a variety of optical systems leading to a number of unusual wave phenomena and novel applications such as the revival of lasing [14–16], enhanced sensing [17,18], stopping light pulses [19], single-mode lasers [20], unidirectional invisibility [21], and thresholdless $\mathcal{PT}$ transitions [22,23].

Due to the outgoing radiation conditions, the eigenvalue problem of resonant modes on open structures is non-Hermitian, even if the dielectric function ε of the structure is real and positive. Therefore, EPs of resonant modes could exist on properly designed passive structures. For example, a microtoroid cavity with two nearby nanoscale scatterers was designed to have an EP, and it was used to enhance sensing [18]. Periodic structures surrounded by or sandwiched between free space are also open structures. Thus, the eigenvalue problem for resonant modes on such a periodic structure is non-Hermitian and there could be EPs. In fact, EPs have been observed on photonic crystal slabs [24–26], and they exist for any specified wave-vector direction, as far as the geometric parameters are properly chosen [24]. In addition, paired EPs can give rise to bulk Fermi arcs and polarization half-integer topological charges [26].

To reveal the novel properties of EPs on open dielectric structures and realize their potential applications, it is necessary to carry out systematic studies on EPs. In this paper, we develop an efficient numerical method for computing second-order (i.e., doubly degenerate) EPs based on the square-root splitting of the eigenvalues, calculate the EPs on a simple dielectric periodic slab, and find out how they vary with geometric parameters. Although the structure is very simple, many EPs exist, and they exhibit rather complicated dependencies on the parameters. However, we find a simple analytic result for the limit as the periodic slab approaches a uniform slab. The EPs in this limit are related to artificial degeneracies of the guided modes of the uniform slab when it is regarded as a periodic slab. The rest of this paper is organized as follows: In Sec. II, we give some definitions and show the band structure of a particular periodic slab. In Sec. III, we develop an efficient numerical method for computing EPs and show the band structure of a periodic slab with one EP. In Sec. IV, we analyze the artificial degeneracies of a uniform slab. In Sec. V, we calculate the EPs on the periodic slab and show their dependence on parameters, including the limit studied in Sec. IV. Finally, we conclude our paper with some remarks in Sec. VI.

II. RESONANT MODES

A typical periodic dielectric slab is shown in Fig. 1. The structure is invariant in x, periodic in y with period d, finite in z with a thickness h, and surrounded by air. It is further assumed that each period of the slab consists of two segments with dielectric constants ε_1 and ε_2, and widths a and $d-a$, respectively. For the E polarization, the x component of the electric field, denoted u, satisfies the following two-dimensional (2D) Helmholtz equation:

$$\partial_y^2 u + \partial_z^2 u + k^2 \varepsilon(y,z) u = 0, \tag{1}$$

*Corresponding author: mayylu@cityu.edu.hk

 ©2018 American Physical Society

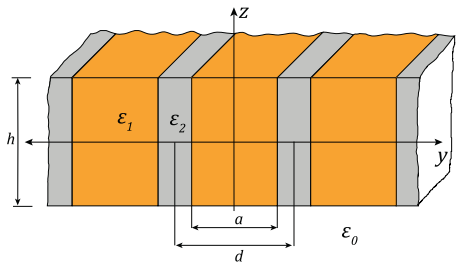

FIG. 1. A dielectric slab invariant in x and periodic in y. Each period consists of two segments.

where $\varepsilon = \varepsilon(y,z)$ is the dielectric function of the structure, $k = \omega/c$ is the free-space wave number, ω is the angular frequency, and c is the speed of light in vacuum.

A Bloch mode on the periodic slab is a solution of Eq. (1) given in the form

$$u(y,z) = \phi(y,z)\, e^{i\beta y}, \tag{2}$$

where β is a real Bloch wave number satisfying $|\beta| \leqslant \pi/d$, and $\phi(y,z)$ is periodic in y with period d. In the free space surrounding the slab, i.e., for $|z| > h/2$, the solution can be expanded in plane waves as

$$u(y,z) = \sum_{m=-\infty}^{\infty} \hat{u}_m^{\pm} e^{i(\beta_m y \pm \alpha_m z)}, \quad \pm z > h/2, \tag{3}$$

where $\hat{u}_m^{\pm}$ are the expansion coefficients,

$$\beta_m = \beta + 2\pi m/d, \quad \alpha_m = \sqrt{k^2 - \beta_m^2}, \tag{4}$$

and the square root is defined with a branch cut along the negative imaginary axis.

If $\phi(y,z) \to 0$ as $|z| \to \infty$, then the Bloch mode is a guided mode. Below the light line, i.e., for $k < |\beta|$, guided modes exist continuously with respect to frequency and wave number. Above the light line, Bloch modes with the expansion (3) are typically resonant modes with a complex frequency; that is, k is complex and $\mathrm{Re}(k) > |\beta|$. The resonant modes satisfy outgoing radiation conditions as $|z| \to \infty$. From Eq. (4), it is clear that α_0 is a complex number with a negative imaginary part. Therefore, the plane waves $\exp[i(\beta y \pm \alpha_0 z)]$ blow up as $z \to \pm\infty$, respectively. The quality factor, denoted Q, of a resonant mode is given by $Q = -0.5\,\mathrm{Re}(k)/\mathrm{Im}(k)$. In special circumstances, resonant modes with infinite quality factors, i.e., $\mathrm{Im}(k) = 0$, may exist, and they are the bound states in the continuum (BICs). The BICs have intriguing properties and important applications [27].

Numerical methods for computing the Bloch modes can be classified as time-domain methods such as finite-difference time domain [28], and frequency-domain methods including both linear and nonlinear schemes. A linear scheme discretizes the Helmholtz equation directly to obtain a linear matrix eigenvalue problem for eigenvalue k^2. A nonlinear scheme produces a nonlinear eigenvalue problem with a smaller matrix whose entries depend on k implicitly. The mode-matching method is a nonlinear scheme. For the structure shown in Fig. 1, it gives rise to a homogeneous linear system $\boldsymbol{A}(\beta,k)\boldsymbol{x} = \boldsymbol{0}$, where $\boldsymbol{x}$ is a vector of unknown expansion coefficients. For a given β, nontrivial solutions can be found by searching complex k such that $\lambda_1(\boldsymbol{A}) = 0$, where $\lambda_1(\boldsymbol{A})$ is the eigenvalue of $\boldsymbol{A}$ with the smallest magnitude. Additional details about the numerical methods are given in Appendix.

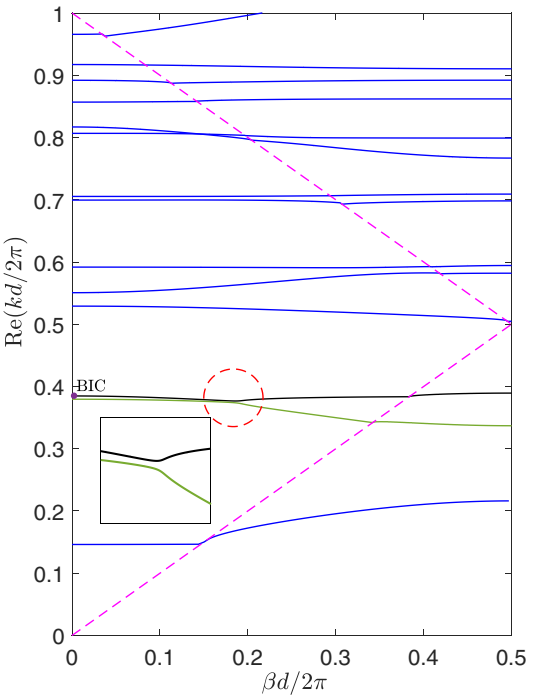

FIG. 2. Band structure of Bloch modes (odd in z) on a periodic slab with $\varepsilon_1 = 15.42$, $\varepsilon_2 = 1$, $a = 0.5d$, and $h = 1.16d$.

As a numerical example, we show the band structure of a periodic slab with $\varepsilon_1 = 15.42$, $\varepsilon_2 = 1$, $a = 0.5d$, and $h = 1.16d$ in Fig. 2. To obtain these results, we first use a linear scheme to calculate the eigenmodes at $\beta = 0$, and then use the more accurate mode-matching method to find each band for $0 < \beta \leqslant \pi/d$. For simplicity, we only show $\mathrm{Re}(k)$ for resonant modes that are odd functions of z. Notice that two curves, the solid black one and the solid green one, are close to each other at $\beta \approx 0.18(2\pi/d)$. In Fig. 3, we show the quality factors of the resonant modes corresponding to these two curves. It can be seen that the quality factors are also close to each other at $\beta \approx 0.18(2\pi/d)$. Notice that the quality factor of the black curve diverges at $\beta = 0$, and this corresponds to a BIC at $\beta = 0$, i.e., a standing wave. Meanwhile, the quality factors of both curves diverge as the pair (β,k) approaches the light line.

In the next section, we show that by tuning one structural parameter, these two resonant modes can be forced to coalesce, giving rise to a second-order EP.

III. EXCEPTIONAL POINTS

If two eigenvalues, say k_+ and k_-, are close to each other for some β, there may be an EP on a structure with slightly different parameters. To find the EP, we can try to find the parameter values and β, such that $k_+ = k_-$, and check whether the eigenfunctions also coalesce. This approach is tedious and inefficient. In the following, we develop an efficient method based on the square-root splitting of the eigenvalues at second-order EPs.

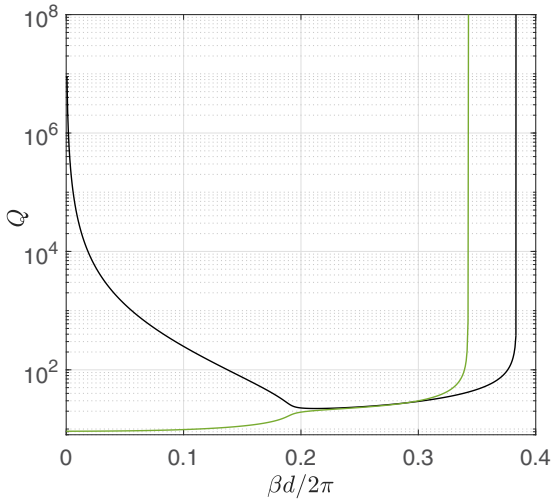

FIG. 3. Quality factors of the resonant modes corresponding to the black and green curves in Fig. 2.

Let k_* and β_* be the eigenvalue and Bloch wave number of a second-order EP associated with the bands $k_+(\beta)$ and $k_-(\beta)$. In the vicinity of the EP, the eigenvalues have the following approximations:

$$k_\pm(\beta) \approx k_* \pm (b_1 + i\, b_2)\sqrt{\beta - \beta_*}, \quad \beta > \beta_*, \tag{5}$$

$$k_\pm(\beta) \approx k_* \pm (c_1 + i\, c_2)\sqrt{\beta_* - \beta}, \quad \beta < \beta_*, \tag{6}$$

where b_1, b_2, c_1, and c_2 are unknown real constants. Since the EP is a resonant mode with $\beta = \beta_*$ and $k = k_*$, we have

$$\lambda_1[\boldsymbol{A}(\beta_*,k_*)] = 0, \tag{7}$$

where $\boldsymbol{A}(\beta,k)$ is a matrix obtained by the mode-matching method (see Appendix). In addition, for a small $\delta\beta > 0$, two resonant modes exist at $\beta = \beta_* + \delta\beta$ with $k_\pm(\beta)$ given by Eq. (5). This leads to

$$\lambda_1[\boldsymbol{A}(\beta_* + \delta\beta, k_* + \delta k)] \approx 0, \tag{8}$$

$$\lambda_1[\boldsymbol{A}(\beta_* + \delta\beta, k_* - \delta k)] \approx 0, \tag{9}$$

where $\delta k = (b_1 + ib_2)\sqrt{\delta\beta}$. Therefore, we can find second-order EPs by choosing a proper $\delta\beta$ and solving Eqs. (7)–(9). It turns out that EPs can be found by tuning just one structural parameter. If ε_1, ε_2, and a are fixed, we can search the slab thickness h to find EPs. The three complex equations (7)–(9), corresponding to six real equations, are used to determine six real unknowns: $\{h_*, \beta_*, \mathrm{Re}(k_*), \mathrm{Im}(k_*), b_1, b_2\}$, where h_* denotes the particular value of h for EPs. The values of b_1 and b_2 describe how strongly the modes split from the EP as β moves away from β_*.

Following the example in Sec. II, we choose $\varepsilon_1 = 15.42$, $\varepsilon_2 = 1$, and $a = 0.5d$ and allow h to vary. Using the method described above, we found an EP for $h_* = 1.154\,485d$, $\beta_* = 0.187\,005(2\pi/d)$, and $k_* = (0.376\,190\,4 - 0.009\,219\,4i)\,(2\pi/d)$. The band structure of the periodic slab with thickness h_* is shown in Fig. 4. It is clear that two two bands touch at the EP with a square-root splitting in the vicinity

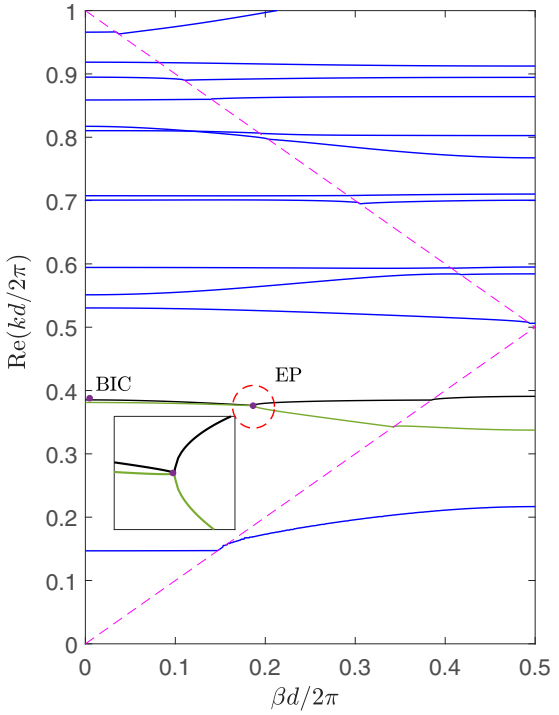

FIG. 4. Band structure of Bloch modes on a periodic slab with $\varepsilon_1 = 15.42$, $\varepsilon_2 = 1$, $a = 0.5d$, and $h_* = 1.154\,485d$.

of β_*. The quality factors of these two bands are shown in Fig. 5. As expected, the two curves in Fig. 5 also touch at β_*.

It should be pointed out that an EP can be calculated by using either Eq. (5) or Eq. (6). For the latter case, we choose a negative $\delta\beta$ and calculate the constants c_1 and c_2. It turns out that these constants satisfy

$$c_1 = \pm b_2 \quad \text{and} \quad c_2 = \mp b_1. \tag{10}$$

More features of the EPs can be understood by closely examining the behavior of the eigenmodes in the vicinity of β_*. In Fig. 6(a), we show the real and imaginary parts of k for two resonant modes around the EP. In Figs. 6(c) and 6(d),

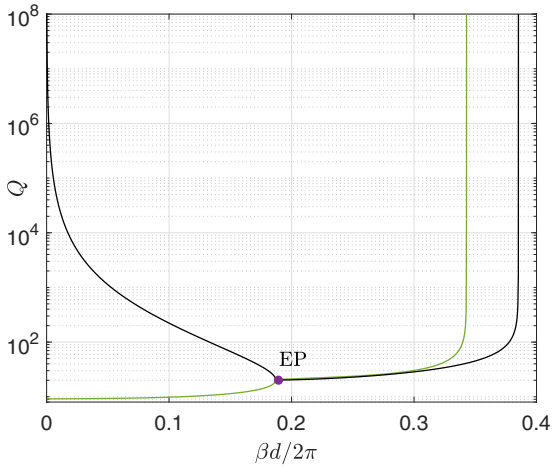

FIG. 5. Quality factors of the resonant modes corresponding to black and green curves in Fig. 4.

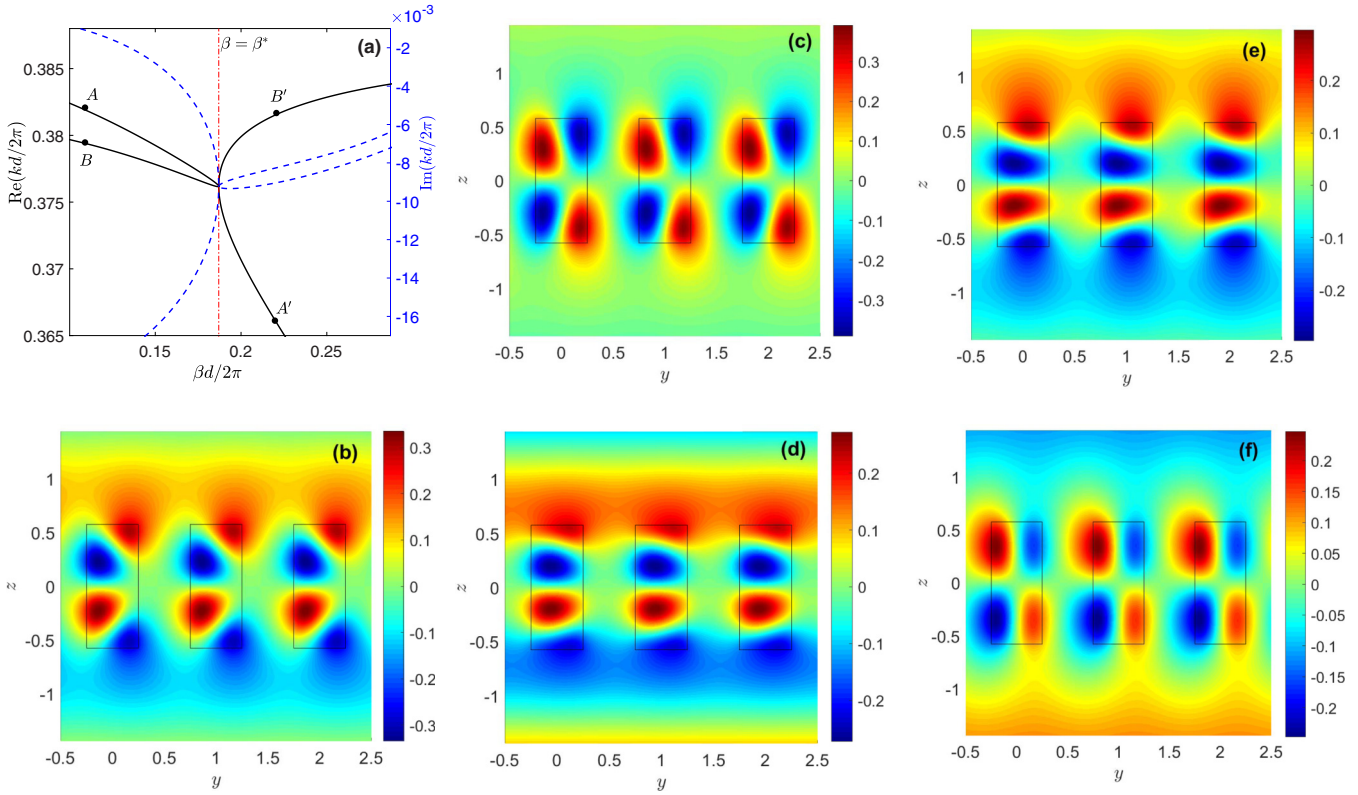

FIG. 6. (a) Dispersion curves around an EP with $\beta_* = 0.187\,005\,(2\pi/d)$. (b) The eigenfunction of the EP solution. (c)–(f) The eigenfunctions at points A, B, B', A' shown in panel (a), respectively.

we show the two eigenfunctions, ϕ_+ and ϕ_-, corresponding to points A and B in Fig. 6(a), respectively. As $\beta \to \beta_*$, those two eigenfunctions coalesce into a single EP eigenfunction ϕ_* as shown in Fig. 6(b). Notice that the field pattern of ϕ_* combines the main features of ϕ_- and ϕ_+. For $\beta > \beta_*$, two different eigenfunctions are recovered, and they are shown in Figs. 6(e) and 6(f), corresponding to points B' and A' in Fig. 6(a), respectively. Notice that the field patterns for points A and A' are similar, and those for B and B' are also similar, but their ordering with respect to $\mathrm{Re}(k)$ is reversed. This switching behavior of the field patterns as β passes through β_* is consistent with Eq. (10).

To develop a better understanding about EPs on the periodic slab, we analyze their dependence on parameter a in Sec. V. It will be shown that these EPs continue to exist as $a \to d$, and their β_* and k_* approach the light line. It also appears that the limiting points on the light line are related to some artificial degeneracies of the uniform slab when it is regarded as a periodic structure. Artificial degeneracies in band structures also appear when a periodic structure with a certain period is regarded as one with a larger period, and they are related to thresholdless $\mathcal{PT}$ transitions in 2D photonic crystals [22]. In the next section, we study the artificial degeneracies of a uniform slab and calculate the limiting points on the light line.

IV. UNIFORM SLAB

Referring to Fig. 1, by setting $a = d$, we have a uniform slab with $\varepsilon = \varepsilon_1$. A guided mode is now given by

$$u(y,z) = \tilde{\phi}(z)e^{i\tilde{\beta}y}, \tag{11}$$

where $\tilde{\beta}$ is the propagation constant, and $\tilde{\phi}$ satisfies

$$\frac{d^2\tilde{\phi}}{dz^2} + k^2\varepsilon(z)\tilde{\phi} = \tilde{\beta}^2\tilde{\phi}, \tag{12}$$

where $\varepsilon(z) = \varepsilon_1$ for $|z| < h/2$ and $\varepsilon(z) = 1$ for $|z| > h/2$. In addition, $\tilde{\phi}$ must decay to zero as $|z| \to \infty$. As in previous sections, we only consider the modes that are odd in z and denote their dispersion relations as $k = k_m(\tilde{\beta})$ for positive integers m. It is straightforward to show that these dispersion

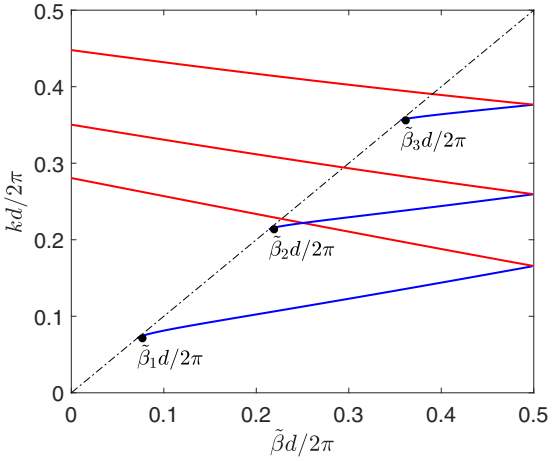

FIG. 7. Folded band structure of a uniform slab with $h = 1.85d$.

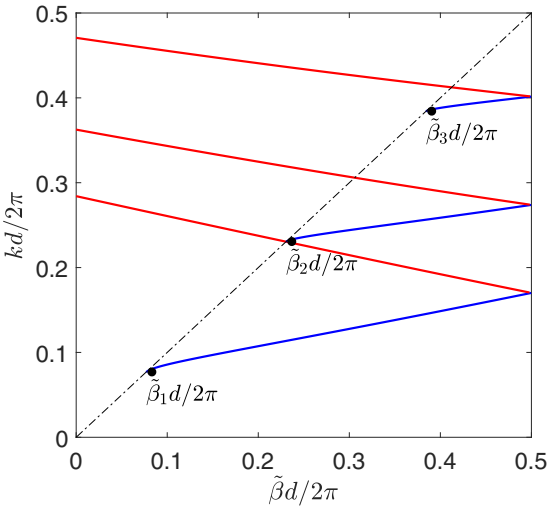

FIG. 8. Folded band structure of a uniform slab with $h = 1.713\,719\,2d$.

curves touch the light line when

$$\tilde{\beta} = k_m(\tilde{\beta}) = \tilde{\beta}_m \triangleq \frac{2\pi(m-1/2)}{h\sqrt{\varepsilon_1 - 1}}. \tag{13}$$

The uniform slab can be regarded as a periodic structure with a *fictitious* period d, then the guided modes can be written as $u(y,z) = \phi(y,z)\exp(i\beta y)$, where

$$\phi(y,z) = \tilde{\phi}(z)e^{i2\pi l\, y/d}, \quad \beta = \tilde{\beta} - 2\pi l/d,$$

for some integer l such that $\beta \in [-\pi/d, \pi/d]$. If $|\tilde{\beta}| \leqslant \pi/d$, then $l = 0$ and $\beta = \tilde{\beta}$. Otherwise, l is nonzero and the dispersion curves of the fictitious periodic slab can be obtained by folding the dispersion curves of the uniform slab into the first Brillouin zone. This is shown in Fig. 7 for $h = 1.85d$, where the solid blue and red curves correspond to $l = 0$ and $l = 1$, respectively. More precisely, the sold red curves are

$$k = k_m^{(\mathrm{f})}(\beta) \triangleq k_m(2\pi/d - \beta).$$

For the case shown in Fig. 7, the dispersion curves have no intersections on the light line. However, it is possible to have intersections on the light line if we tune the value of h. In general, we have the following "limiting degeneracy problem":

TABLE I. Solutions of the "limiting degeneracy problem."

(m,n)	h_*/d	$k_* d/2\pi$
(2,1)	1.7137192	0.2304989
(3,1)	3.0874410	0.2132351
(3,2)	2.5587359	0.2572953
(4,1)	4.4232537	0.2083741
(4,2)	4.0470027	0.2277466
(4,3)	3.3127043	0.2782292
(5,1)	5.7438584	0.2063128
(5,2)	5.4487877	0.2174853
(5,3)	4.9112722	0.2412881
(5,4)	4.0155953	0.2951073

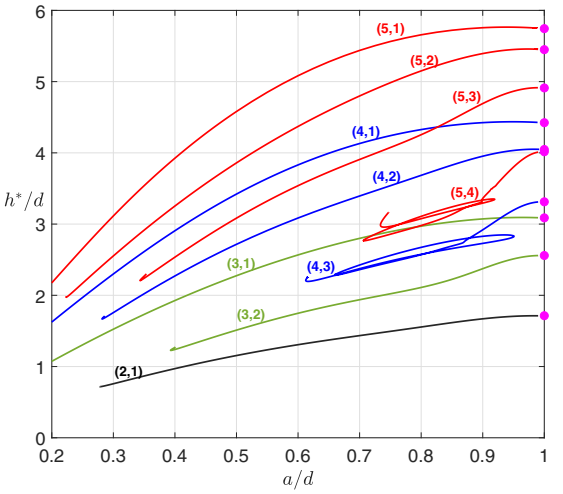

FIG. 9. Slab thickness h_* versus width a for EPs satisfying $\beta_* < \mathrm{Re}(k_*) < 2\pi/d - \beta_*$. The limiting values of these curves as $a/d \to 1$ correspond to those h_* listed in Table I.

Given integers $m > n > 0$, find h_* such that

$$k_n(2\pi/d - \tilde{\beta}_m) = \tilde{\beta}_m. \tag{14}$$

For $m = 2$ and $n = 1$, we solve the above problem and obtain $h_* = 1.713\,719\,2d$. In Fig. 8, the dispersion curves are shown for this h_*, and the intersection on the light line is $k_* = \beta_* = 0.230\,498\,9\,(2\pi/d)$. The results for different pairs (m,n) are listed in Table I.

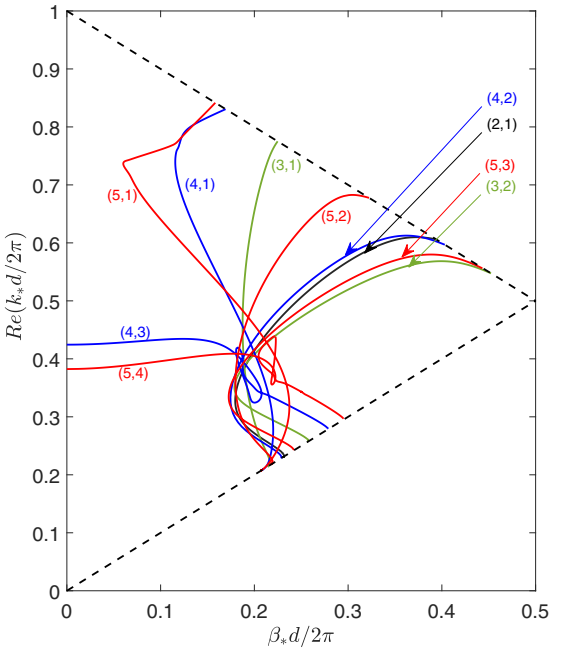

FIG. 10. Eigenvalue k_* versus wave number β_* for the same EPs as shown in Fig. 9. The curves tend to the light line as $a \to d$, and the points on the light line correspond to those k_* given in Table I.

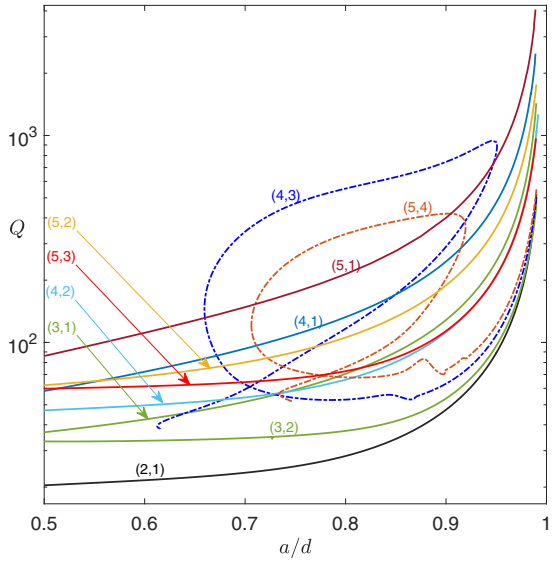

FIG. 11. Quality factors versus a for the same EPs as shown in Fig. 9. The quality factors diverge as $a \to d$.

V. CONTINUATION OF EXCEPTIONAL POINTS

In Sec. III, we presented one EP for a periodic slab with $a = 0.5d$. In fact, many different EPs can be found for the same a, but typically for different slab thickness. To get a more complete picture about the EPs on the periodic slab, we use the numerical method of Sec. III to follow the EPs in the parameter space of a and h, while keeping $\varepsilon_1 = 15.42$ and $\varepsilon_2 = 1$ fixed. For simplicity, only those resonant modes that are odd in z are considered. The results are shown in Figs. 9–11 for h_* vs a, $\mathrm{Re}(k_*)$ vs β_*, and quality factor vs a, respectively.

In Fig. 9, we show ten curves in the a-h plane, where each curve represents one family of EPs that depend continuously on a and h. These curves are labeled by pairs of integers (m,n). Notice that as $a \to d$, all these curves tend to the values of h_* listed in Table I, according to their corresponding labels. The β_* and k_* values of the ten families of EPs are shown in Fig. 10. As $a \to d$, the curves in Fig. 10 approach the light line exactly at the values of k_* listed in Table I. Therefore, it can be argued that all these EPs *originate* from the artificial degeneracies of the guided modes on the uniform slab. In Fig. 9, we observe that different curves, e.g., (4,1) and (5,3), may intersect. This simply means that, for the same periodic slab, there are two EPs with different β_* and k_*. Notice that the curves (4,3) and (5,4) can intersect with themselves. On a periodic slab corresponding to such an intersection, there are two EPs that belong to the same family, but their β_* and k_* are again different. The left endpoints of the curves in Fig. 9 correspond to either $\beta_* = 0$, or $\beta_* = 2\pi/d - \mathrm{Re}(k_*)$ which is the opening line of the second radiation channel. EPs exist

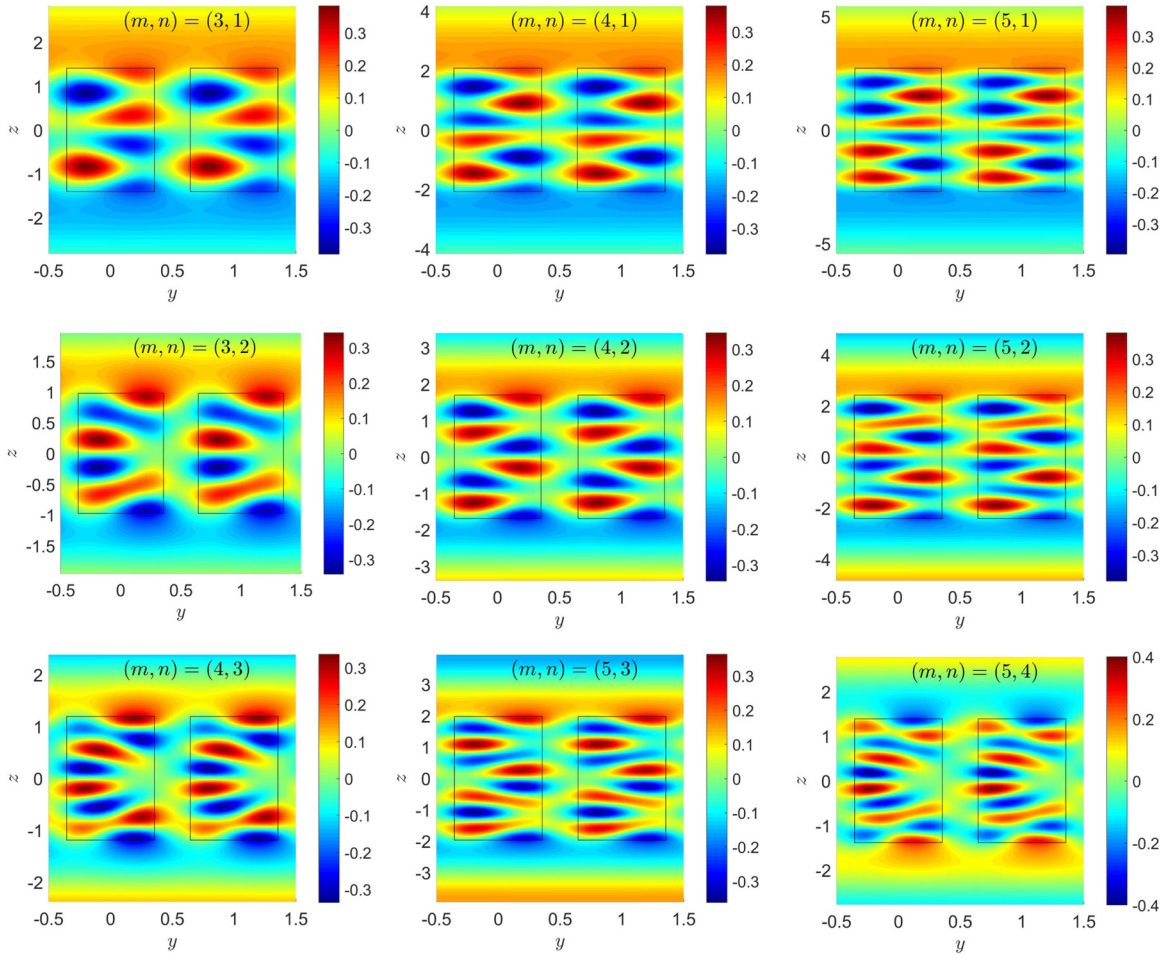

FIG. 12. Eigenfunctions ϕ_* for EPs on periodic slabs with $a = 0.7d$ and different h_*. The EPs are labeled by integer pairs (m,n) as in Fig. 9.

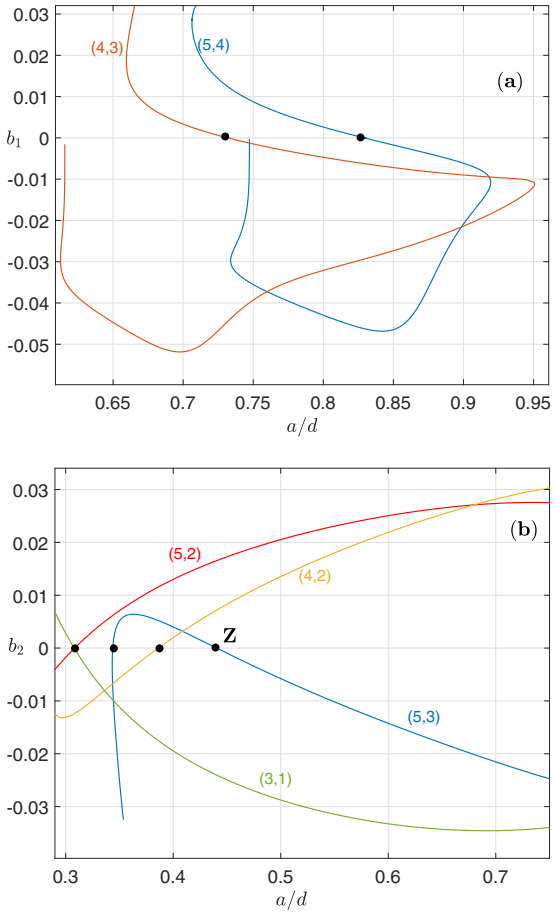

FIG. 13. (a) Coefficient b_1 versus a. (b) Coefficient b_2 versus a. Solid black dots are zeros of b_1 or b_2.

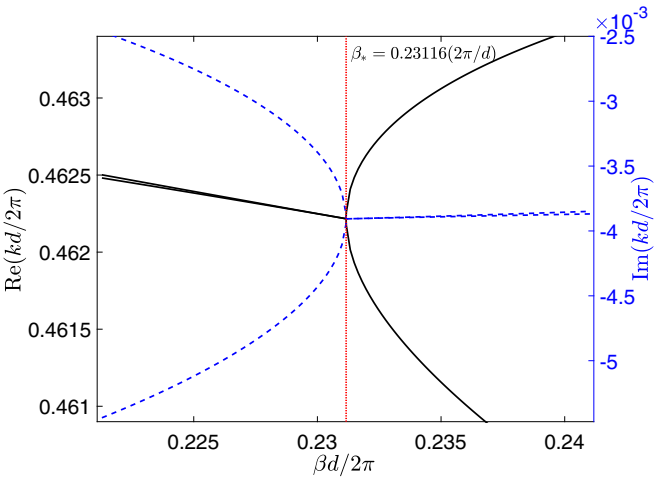

FIG. 14. One-sided square-root splitting of Re(k) (solid black curves) and Im(k) (dashed blue curves) for an EP with $b_2 = 0$, i.e., point Z in Fig. 13(b).

beyond this line, but they tend to have lower quality factors. The quality factors of the ten families of EPs are shown in Fig. 11. It can be observed that the quality factors of all EPs diverge as $a \to d$, and they are relatively small for smaller values of a.

In Fig. 12, we show the field patterns of nine EPs on periodic slabs with $a = 0.7d$. The case for $(m,n) = (2,1)$ is not shown, since it is similar to the one in Fig. 6(b) for $a = 0.5d$. Notice that different scales in z are used in the different panels, since the values of h_* are different for different EPs. It should be pointed out that the wave field pattern varies continuously on each curve shown in Fig. 9, and the main features, such as the number of polarity changes along the y and z axes, are preserved when (a,h_*) moves along each curve.

Near a second-order EP, the dispersion curves exhibit a square-root splitting. One example is shown in Fig. 6(a), where a square-root splitting can be observed for both real and imaginary parts of k, and for both $\beta > \beta_*$ and $\beta < \beta_*$. For this particular case, Re(k) has a stronger splitting for $\beta > \beta_*$, and Im(k) has a stronger splitting for $\beta < \beta_*$, since $|b_1| = |c_2| > |b_2| = |c_1|$. For some special EPs, b_1 or b_2 can be exactly zero. In Figs. 13(a) and 13(b), we show b_1 and b_2 vs a for a few families of EPs. It is clear that b_1 or b_2 can be zero for some special values of a. If b_1 or b_2 is zero, the square-root splitting becomes one-sided. For example, if $b_2 = c_1 = 0$, then Re(k) has a square-root splitting only for $\beta > \beta_*$, and Im(k) has a square-root splitting only for $\beta < \beta_*$. A particular example is shown in Fig. 14 and corresponds to point Z marked in Fig. 13(b). Actually, although $b_2 = 0$, Im(k) still shows a splitting for $\beta > \beta_*$, but it is a weaker linear splitting proportional to $\beta - \beta_*$. The same is true for Re(k) and $\beta < \beta_*$.

VI. CONCLUSION

Electromagnetic resonant modes on open dielectric structures are solutions of a non-Hermitian eigenvalue problem derived from the Maxwell's equations. EPs of resonant modes are special degenerate states for which both the eigenvalues and the eigenfunctions coalesce. In optical systems, EPs have given rise to many interesting wave phenomena and some important applications. In this paper, we investigated exceptional points on a simple dielectric periodic slab. An efficient numerical method for computing second-order EPs was developed and used to calculate families of EPs that vary continuously with structural parameters. Due to the extra degree of freedom related to the Bloch wave number, it is possible to find EPs by tuning only one parameter of the periodic structure. It is worth mentioning that analytic results have been obtained for the limit $a \to d$, i.e., the periodic slab approaching a uniform one. It was shown that the EPs tend to some points on the light line in this limit, and these points are related to some artificial degeneracies of the band structure of a uniform slab when it is regarded as a periodic one.

Our results show that the EPs have rather complicated dependence on the geometric parameters of the periodic slab. For simplicity, we have concentrated on the odd resonant modes in the E polarization for a very simple periodic slab. Further studies are needed to understand EPs on more general and three-dimensional structures, to reveal their properties including existence and robustness, to find out their impact on transmission spectra, reflection spectra and field enhancement, and to realize more valuable applications.

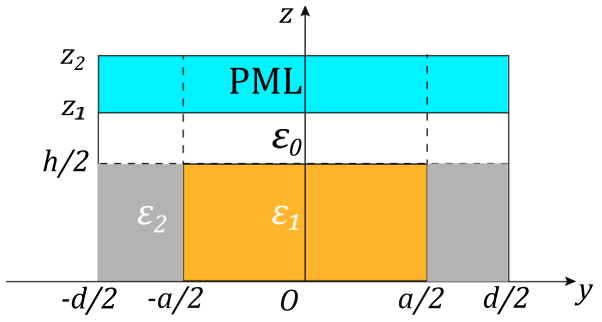

FIG. 15. One period of the periodic slab divided into subdomains of constant permittivity.

ACKNOWLEDGMENTS

The second author acknowledges support from the Research Grants Council of Hong Kong Special Administrative Region, China (Grant No. CityU 11304117).

APPENDIX: NUMERICAL METHODS

The eigenvalue problem for resonant modes on the periodic slab can be solved by a linear scheme based on the Chebyshev pseudospectral method [29] and the perfectly matched layer (PML) technique [30,31]. For the periodic function ϕ given in Eq. (2), the Helmholtz equation (1) becomes

$$\frac{\partial^2\phi}{\partial z^2}+\frac{\partial^2\phi}{\partial y^2}+2i\beta\frac{\partial\phi}{\partial y}-\beta^2\phi=-k^2\varepsilon\phi. \tag{A1}$$

If the modes are odd in z, it is only necessary to consider $z>0$ together with a zero boundary condition at $z=0$. The z axis is truncated at $z=z_2$ with a PML for $z_1<z<z_2$, as shown in Fig. 15. The PML replaces z by $\hat{z}$ or dz by $d\hat{z}=s(z)dz$ for a complex function $s(z)$. Hence, Eq. (A1) becomes

$$\frac{1}{s(z)}\frac{\partial}{\partial z}\left[\frac{1}{s(z)}\frac{\partial\phi}{\partial z}\right]+\frac{\partial^2\phi}{\partial y^2}+2i\beta\frac{\partial\phi}{\partial y}-\beta^2\phi=-k^2\varepsilon\phi. \tag{A2}$$

In addition, ϕ must satisfy the boundary conditions

$$\phi(y,0)=\phi(y,z_2)=0, \tag{A3}$$

and periodic conditions

$$\phi(-d/2,z)=\phi(d/2,z), \tag{A4}$$

$$\frac{\partial\phi}{\partial y}(-d/2,z)=\frac{\partial\phi}{\partial y}(d/2,z). \tag{A5}$$

We use the Chebyshev pseudospectral method [29] to discretize Eq. (A2) on each rectangular subdomain shown in Fig. 15 and impose field continuity conditions and conditions (A3)–(A5) on the boundaries of the subdomains. The result is a linear matrix eigenvalue problem of the form

$$\boldsymbol{L\phi}=k^2\boldsymbol{\phi}, \tag{A6}$$

where $\boldsymbol{\phi}$ is a vector containing the values of ϕ at the interior Chebyshev collocation points.

The eigenvalue problem for resonant modes on the periodic slab can also be solved by a nonlinear scheme based on the mode-matching method. For the odd (in z) modes, the structure is divided into two layers given by $0<z<h/2$ and $z>h/2$, and the dielectric function is $\varepsilon^{(1)}(y)$ and $\varepsilon^{(2)}(y)$ in these two layers, respectively. For given β and k, we can expand ϕ in each layer in one-dimensional eigenmodes. The eigenvalue problem in the lth layer is

$$\left[\frac{d^2}{dy^2}+2i\beta\frac{d}{dy}+k^2\varepsilon^{(l)}(y)-\beta^2\right]\psi^{(l)}=[\eta^{(l)}]^2\psi^{(l)},$$

subject to the periodic boundary conditions

$$\psi^{(l)}(-d/2)=\psi^{(l)}(d/2),$$
$$\frac{d\psi^{(l)}}{dy}(-d/2)=\frac{d\psi^{(1)}}{dy}(d/2).$$

Solving the above by the Chebyshev collocation method [29], we obtain

$$\left\{\psi_j^{(l)},\eta_j^{(l)}\right\}_{j=1}^{N},\quad l=1,2,$$

for a positive integer N and discretization points $\{y_p\}_{p=1}^{N}$.

With the above eigenmodes, ϕ can be expanded as

$$\phi(y,z)=\sum_{j=1}^{N}\frac{c_j\sin\left(\eta_j^{(1)}z\right)}{\sin\left(0.5\eta_j^{(1)}h\right)}\psi_j^{(l)}(y),\quad 0\leqslant z<\frac{h}{2},$$
$$\phi(y,z)=\sum_{j=1}^{N}d_je^{i\eta_j^{(2)}(z-h/2)}\psi_j^{(2)}(y),\quad z>\frac{h}{2}.$$

Enforcing the continuity of ϕ and $\partial_z\phi$ at $y=y_p$ and $z=h/2$ for $1\leqslant p\leqslant N$, we obtain the following linear system:

$$\boldsymbol{A}\begin{bmatrix}\mathbf{c}\\ \mathbf{d}\end{bmatrix}=\begin{bmatrix}\boldsymbol{A}_{11}&\boldsymbol{A}_{12}\\ \boldsymbol{A}_{21}&\boldsymbol{A}_{22}\end{bmatrix}\begin{bmatrix}\boldsymbol{c}\\ \boldsymbol{d}\end{bmatrix}=\mathbf{0}, \tag{A7}$$

where $\boldsymbol{c}$ and $\boldsymbol{d}$ are column vectors of c_j and d_j $(1\leqslant j\leqslant N)$, respectively, $\boldsymbol{A}$ is a 2×2 block matrix depending on β and k, and the (p,j) entries of the matrix blocks are

$$\boldsymbol{A}_{11}(p,j)=\psi_j^{(1)}(y_p),$$
$$\boldsymbol{A}_{12}(p,j)=-\psi_j^{(2)}(y_p),$$
$$\boldsymbol{A}_{21}(p,j)=\eta_j^{(1)}\cot\left(0.5\eta_j^{(1)}h\right)\psi_j^{(1)}(y_p),$$
$$\boldsymbol{A}_{22}(p,j)=-i\eta_j^{(2)}\psi_j^{(2)}(y_p).$$

Equation (A7) has a nontrivial solution, only when $\boldsymbol{A}$ is singular. Therefore, we can find the complex k from the condition $\lambda_1(\boldsymbol{A})=0$, where $\lambda_1(A)$ is the eigenvalue of $\boldsymbol{A}$ with the smallest magnitude.

[1] T. Kato, *Perturbation Theory for Linear Operators* (Springer, Berlin, 1966).

[2] N. Moiseyev, *Non-Hermitian Quantum Mechanics* (Cambridge University Press, New York, 2011).

[3] W. D. Heiss, The physics of exceptional points, J. Phys. A: Math. Theor. **45**, 444016 (2012).

[4] C. A. Jones, Multiple eigenvalues and mode classification in plane Poiseuille flow, Q. J. Mech. Appl. Math. **41**, 363 (1988).

[5] W. D. Heiss and A. L. Sannino, Avoided level crossing and exceptional points, J. Phys. A: Math. Gen. **23**, 1167 (1990).

[6] W. D. Heiss and A. L. Sannino, Transitional regions of finite Fermi systems and quantum chaos, Phys. Rev. A **43**, 4159 (1991).

[7] F. Leyvraz and W. D. Heiss, Large-n Scaling Behavior of the Lipkin-Meshkov-Glick Model, Phys. Rev. Lett. **95**, 050402 (2005).

[8] H. Cartarius, J. Main, and G. Wunner, Discovery of exceptional points in the Bose-Einstein condensation of gases with attractive $1/r$ interaction, Phys. Rev. A **77**, 013618 (2008).

[9] C. M. Bender and S. Boettcher, Real Spectra in Non-Hermitian Hamiltonians having $\mathcal{PT}$ Symmetry, Phys. Rev. Lett. **80**, 5243 (1998).

[10] C. M. Bender, S. Boettcher, and P. N. Meisinger, PT-symmetric quantum mechanics, J. Math. Phys. **40**, 2201 (1999).

[11] C. M. Bender, M. V. Berry, and A. Mandilara, Generalized PT symmetry and real spectra, J. Phys. A: Math. Gen. **35**, L467 (2002).

[12] S. Klaiman, U. Günther, and N. Moiseyev, Visualization of Branch Points in $\mathcal{PT}$-Symmetric Waveguides, Phys. Rev. Lett. **101**, 080402 (2008).

[13] C. E. Rüter, K. G. Makris, R. El-Ganainy, D. N. Christodoulides, M. Segev, and D. Kip, Observation of parity-time symmetry in optics, Nat. Phys. **6**, 192 (2010).

[14] M. Liertzer, L. Ge, A. Cerjan, A. D. Stone, H. E. Türeci, and S. Rotter, Pump-Induced Exceptional Points in Lasers, Phys. Rev. Lett. **108**, 173901 (2012).

[15] B. Peng, Ş. K. Özdemir, S. Rotter, H. Yilmaz, M. Liertzer, F. Monifi, C. M. Bender, F. Nori, and L. Yang, Loss-induced suppression and revival of lasing, Science **346**, 328 (2014).

[16] M. Brandstetter, M. Liertzer, C. Deutsch, P. Klang, J. Schöberl, H. E. Türeci, G. Strasser, K. Unterrainer, and S. Rotter, Reversing the pump dependence of a laser at an exceptional point, Nat. Commun. **5**, 4034 (2014).

[17] H. Hodaei, A. U. Hassan, S. Wittek, H. Garcia-Gracia, R. El-Ganainy, D. N. Christodoulides, and M. Khajavikhan, Enhanced sensitivity at higher-order exceptional points, Nature (London) **548**, 187 (2017).

[18] W. Chen, Ş. K. Özdemir, G. Zhao, J. Wiersig, and L. Yang, Exceptional points enhance sensing in an optical microcavity, Nature (London) **548**, 192 (2017).

[19] T. Goldzak, A. A. Mailybaev, and N. Moiseyev, Light Stops at Exceptional Points, Phys. Rev. Lett. **120**, 013901 (2018).

[20] L. Feng, Z. J. Wong, R.-M. Ma, Y. Wang, and X. Zhang, Single-mode laser by parity-time symmetry breaking, Science **346**, 972 (2014).

[21] Z. Lin, H. Ramezani, T. Eichelkraut, T. Kottos, H. Cao, and D. N. Christodoulides, Unidirectional Invisibility Induced by $\mathcal{PT}$-Symmetric Periodic Structures, Phys. Rev. Lett. **106**, 213901 (2011).

[22] A. Cerjan, A. Raman, and S. Fan, Exceptional Contours and Band Structure Design in Parity-Time Symmetric Photonic Crystals, Phys. Rev. Lett. **116**, 203902 (2016).

[23] A. Mock, Parity-time-symmetry breaking in two-dimensional photonic crystals: Square lattice, Phys. Rev. A **93**, 063812 (2016).

[24] B. Zhen, C. W. Hsu, Y. Igarashi, L. Lu, I. Kaminer, A. Pick, S.-L. Chua, J. D. Joannopoulos, and M. Soljacic, Spawning rings of exceptional points out of Dirac cones, Nature (London) **525**, 35 (2015).

[25] P. M. Kamiński, A. Taghizadeh, O. Breinbjerg, J. Mørk, and S. Arslanagić, Control of exceptional points in photonic crystal slabs, Opt. Lett. **42**, 2866 (2017).

[26] H. Zhou, C. Peng, Y. Yoon, C. W. Hsu, K. A. Nelson, L. Fu, J. D. Joannopoulos, M. Soljacic, and B. Zhen, Observation of bulk Fermi arc and polarization half charge from paired exceptional points, Science **359**, 1009 (2018).

[27] C. W. Hsu, B. Zhen, A. D. Stone, J. D. Joannopoulos, and M. Soljačić, Bound states in the continuum, Nat. Rev. Mater. **1**, 16048 (2016).

[28] A. F. Oskooi, D. Roundy, M. Ibanescu, P. Bermel, J. D. Joannopoulos, and S. G. Johnson, Meep: A flexible free-software package for electromagnetic simulations by the FDTD method, Comput. Phys. Commun. **181**, 687 (2010).

[29] L. N. Trefethen, *Spectral Methods in MATLAB* (Society for Industrial and Applied Mathematics, Philadelphia, 2000).

[30] J.-P. Berenger, A perfectly matched layer for the absorption of electromagnetic waves, J. Comput. Phys. **114**, 185 (1994).

[31] W. C. Chew and W. H. Weedon, A 3D perfectly matched medium from modified Maxwell's equations with stretched coordinates, Microwave Opt. Technol. Lett. **7**, 599 (1994).